Zhao *et al. Alzheimer's Research & Therapy* (2025) 17:36
https://doi.org/10.1186/s13195-025-01683-0

Alzheimer's Research & Therapy

RESEARCH Open Access

Multi-omics analyses identify gut microbiota-fecal metabolites-brain-cognition pathways in the Alzheimer's disease continuum

Han Zhao[1,2,3,4†], Xia Zhou[5†], Yu Song[1,2,3,4], Wenming Zhao[1,2,3,4], Zhongwu Sun[5*], Jiajia Zhu[1,2,3,4*] and Yongqiang Yu[1,2,3,4*]

Abstract

Background Gut microbiota dysbiosis is linked to Alzheimer's disease (AD), but our understanding of the molecular and neuropathological bases underlying such association remains fragmentary.

Methods Using 16S rDNA amplicon sequencing, untargeted metabolomics, and multi-modal magnetic resonance imaging, we examined group differences in gut microbiome, fecal metabolome, neuroimaging measures, and cognitive variables across 30 patients with AD, 75 individuals with mild cognitive impairment (MCI), and 61 healthy controls (HC). Furthermore, we assessed the associations between these multi-omics changes using correlation and mediation analyses.

Results There were significant group differences in gut microbial composition, which were driven by 8 microbial taxa (e.g., Staphylococcus and Bacillus) exhibiting a progressive increase in relative abundance from HC to MCI to AD, and 2 taxa (e.g., Anaerostipes) showing a gradual decrease. 26 fecal metabolites (e.g., Arachidonic, Adrenic, and Lithocholic acids) exhibited a progressive increase from HC to MCI to AD. We also observed progressive gray matter atrophy in broadly distributed gray matter regions and gradual micro-structural integrity damage in widespread white matter tracts along the AD continuum. Integration of these multi-omics changes revealed significant associations between microbiota, metabolites, neuroimaging, and cognition. More importantly, we identified two potential mediation pathways: (1) microbiota → metabolites → neuroimaging → cognition, and (2) microbiota → metabolites → cognition.

Conclusion Aside from elucidating the underlying mechanism whereby gut microbiota dysbiosis is linked to AD, our findings may contribute to groundwork for future interventions targeting the microbiota-metabolites-brain-cognition pathways as a therapeutic strategy in the AD continuum.

†Han Zhao and Xia Zhou contributed equally to this work.

*Correspondence:
Zhongwu Sun
sunzhwu@126.com
Jiajia Zhu
zhujiajiagraduate@163.com
Yongqiang Yu
cjr.yuyongqiang@vip.163.com

Full list of author information is available at the end of the article

Keywords Alzheimer's disease, Gut microbiome, Fecal metabolome, Neuroimaging, Cognition

Introduction

Alzheimer's disease (AD) is a neurodegenerative disorder that is the most common cause of dementia and currently has few clinically efficacious disease modifying therapies [1]. The bidirectional interaction between gut microbiota and the brain, i.e., the microbiota-gut-brain axis, has emerged as a topic of active investigation in AD. Gut microbiota is essential for maintaining physical and mental well-being [2], while its dysbiosis may lead to neurodegeneration via disrupting metabolic and immunological processes [3, 4], potentially contributing to the pathogenesis and/or progression of AD [5, 6]. Indeed, both animal and human studies have shown that alterations in the gut microbiome (including microbial diversity and abundance) are linked to AD and its related pathologies [7–13]. Nevertheless, our understanding of the molecular and neuropathological bases that underlie such association remains fragmentary.

Strong evidence has established the fecal metabolome as a functional readout of the gut microbiome [14], such that microbial metabolites could provide a molecular connection between the gut microbiota and the brain [15]. Metabolomics, the high-throughput identification and quantification of small molecules in biological samples, offers a powerful tool to identify novel biomarkers of diseases [16–18]. Recent metabolomics studies have revealed several key metabolic pathways (e.g., ceramide metabolism and acylcarnitine-enriched modules) that are involved in AD [19, 20]. In parallel, advances in magnetic resonance imaging (MRI) techniques and analytic approaches have enabled the in vivo examination of neuropathological changes in the AD continuum [21–24]. Structural, functional, and diffusion MRI can be used to measure gray matter morphology [25, 26], spontaneous intrinsic brain activity [27–29], and white matter integrity [30]. A combined analysis of multi-modal MRI measures would provide integrated information on distinct aspects of the brain [31–35], thereby facilitating a more thorough characterization of AD neuropathology.

In this study, we sought to investigate potential microbiota-metabolites-brain-cognition pathways in the AD continuum. Using a combination of 16S rDNA amplicon sequencing, untargeted metabolomics, and multi-modal MRI, we examined group differences in gut microbiome, fecal metabolome, neuroimaging measures, and cognitive variables across 30 patients with AD, 75 individuals with mild cognitive impairment (MCI), and 61 healthy controls (HC). Furthermore, we assessed the associations between these multi-omics changes using correlation and mediation analyses.

Materials and methods

Participants

All participants (Chinese Han origin, right-handed, aged 50–85 years) were recruited from The First Affiliated Hospital of Anhui Medical University between August 2018 and March 2022. The diagnosis of MCI and probable dementia due to AD was established according to the criteria set forth by the National Institute on Aging Alzheimer's Association (NIA-AA) [36, 37]. The inclusion criteria for MCI were as follows: Montreal Cognitive Assessment (MoCA) scores based on the following educational levels of Chinese people [38]: illiterate individuals ≤ 13, individuals with 1–6 years of education ≤ 19, individuals with 7 or more years of education ≤ 24; Clinical Dementia Rating (CDR) = 0.5 [39]; and essentially preserved daily activities and social functions. Inclusion criteria for AD were as follows: dementia was diagnosed according to the Diagnostic and Statistical Manual of Mental Disorders (DSM-IV) criteria [40]; CDR = 1 or 2 [39]; and dementia due to AD was diagnosed according to the core clinical criteria of probable AD dementia as defined by the NIA-AA criteria. The inclusion criteria for HC were as follows: no complaints of memory loss; MoCA scores: illiterate individuals > 13, individuals with 1–6 years of education > 19, individuals with 7 or more years of education > 24; and CDR = 0. The exclusion criteria were as follows: patients with a history of stroke or the presence of multiple or extensive infarcts or severe white matter hyperintensities; cognitive impairment with other core clinical features such as dementia with Lewy bodies, frontotemporal dementia or other neurological or psychiatric illness; use of medication that could have a substantial effect on cognition; severe liver and kidney diseases, thyroid diseases, tumors, and immune diseases. This study was approved by the Institutional Ethics Committee of The First Affiliated Hospital of Anhui Medical University (20200094) and was conducted following the Declaration of Helsinki. Written informed consent was obtained from all participants after a full explanation of the procedure.

Collection of demographic, clinical, and cognitive data

Demographic and clinical data, including age, sex, years of education, current smoking, alcohol abuse, and comorbidities (hypertension, diabetes mellitus and dyslipidemia), were collected by the researchers during the interview. Each subject's weight and height were measured, and body mass index (BMI) was calculated. Cognitive assessment of all participants was performed by two trained neuropsychological technicians within 1 week of the MRI scan. All participants were evaluated using the

Mini-Mental State Examination (MMSE) [41], MoCA [42], and CDR. Moreover, memory function was further assessed using the 12-words list of the AVLT, including immediate recall (AVLT-IR), short-term delayed recall (5-min delay recall, AVLT-SR), long-term delayed recall (20-min delay recall, AVLT-LR), and recognition [43].

Gut microbiomics analysis

Fecal samples were collected in sterilized tubes and stored immediately in a -80°C freezer within 1 day before or after MRI examination. Gut microbiome was quantified using 16S rDNA amplicon sequencing. Specifically, total genome DNA from the fecal samples was extracted using Cetyltrimethylammonium bromide (CTAB) method. DNA concentration and purity was monitored on 1% agarose gels. To construct the Polymerase Chain Reaction (PCR)-based 16S rDNA amplicon library for sequencing, PCR enrichment of the V4 hypervariable region of 16S rDNA was performed with the forward primer 515F (5′-GTGCCAGCMGCCGCGGTAA-3′) and reverse primer 806R (5′-GGACTACHVGGGTWTCTAAT-3′). Sequencing libraries were generated using TruSeq® DNA PCR-Free Sample Preparation Kit (Illumina, USA) following manufacturer's recommendations and index codes were added. The library quality was assessed on the Qubit@2.0 Fluorometer (Thermo Scientific) and Agilent Bioanalyzer 2100 system. At last, the library was sequenced on an Illumina NovaSeq platform and 250 bp paired-end reads were generated.

We used a standard pipeline for 16S rDNA data analysis [44]. First, the raw paired-end reads were assigned to samples based on their unique barcode sequences. Then, the paired-end reads were merged to obtain raw tags based on the 3' overlapping regions, and barcode and primers are removed. Quality filtering on the raw tags was performed, which would keep reads error rates less than 1%. All of these steps can be completed using VSEARCH (https://github.com/torognes/vsearch), an open source and free of charge multithreaded 64-bit tool for processing and preparing amplicon analysis [45]. To select the representative sequences as proxies of a species, denoising was done by the unoise3 command, which is an implementation of the UNOISE algorithm (http://www.drive5.com/usearch/manual/unoise algo.html). After dereplication, denoised sequences were generated and referred to as amplicon sequence variants (ASV). Finally, reference-based chimera detection was conducted using the Ribosomal Database Project (RDP) as a reference database (http://rdp.cme.msu.edu), and then the ASV table was generated by quantifying the normalized ASV counts in each sample.

Several commonly used gut microbial measures were calculated. First, alpha diversity indices were computed based on the normalized ASV counts using the R package "Vegan" to quantify the level of within-sample diversity in a given fecal sample. We focused our analyses on Shannon and Simpson indices that reflect both species richness and species evenness. Second, beta diversity indices were calculated based on the normalized ASV counts using the USEARCH to quantify the dissimilarity between fecal samples based on Bray-Curtis index and weighted Unifrac distance [46]. Finally, the ASV were assigned taxonomy at the genus level by using RDP as a reference database with a minimum confidence threshold of 0.1, providing a dimensionality reduction perspective on the microbiota. After removing plastid and non-bacteria, microbial relative abundance at the genus level was obtained.

Fecal metabolomics analysis

Fecal metabolome was analyzed using the ultrahigh performance liquid chromatography coupled with tandem mass spectrometry (UHPLC-MS/MS) system [47, 48]. A pooled quality control (QC) sample and instrument blanks were used to assess the reproducibility and to filter out the chemical background contamination. The raw data files were processed by MS-DIAL (version 4.92) [49] with a mass tolerance of 0.01 and 0.025 Da for MS1 and MS2, respectively; the minimum peak height was 50,000, and the identification score cut-off was 70%. For the metabolite identification process, we used the spectral libraries provided by the MS-DIAL team, which incorporate all the available public repositories. The average QC to blank peak area ratio was calculated, and metabolites with a QC/blank peak area ratio < 3 were removed [50]. Signal reproducibility was tested by calculating the relative standard deviation (RSD) of QC sample technical replicates, and metabolites with RSD > 30% were discarded [51]. Metabolites with nonzero measurement in at least 80% of the samples were included [52]. Missing values were replaced by 1/5 of minimum positive values of their corresponding variables. Finally, quantification values of metabolites were normalized by QC samples, made more normally distributed with a generalized log transformation, and standardized using *z*-scores.

MRI data acquisition

MRI scans were obtained using a 3.0-Tesla MR system (Discovery MR750w, General Electric, Milwaukee, WI, USA) with a 24-channel head coil. Earplugs were used to reduce scanner noise, and tight but comfortable foam padding was used to minimize head motion. All participants were instructed to relax, keep their eyes closed but not fall asleep, think of nothing in particular, and move as little as possible. High-resolution 3D T1-weighted structural images were acquired by employing a brain volume (BRAVO) sequence with the following parameters: repetition time (TR) = 8.5 ms; echo time (TE) = 3.2 ms;

inversion time (TI) = 450 ms; flip angle = 12 °; field of view (FOV) = 256 mm × 256 mm; matrix size = 256 × 256; slice thickness = 1 mm, no gap; 188 sagittal slices. Resting-state blood-oxygen level-dependent (BOLD) functional MRI (fMRI) data were acquired using a gradient-echo single-shot echo planar imaging (GRE-SS-EPI) sequence with the following parameters: TR = 2000 ms; TE = 30 ms; flip angle = 90 °; FOV = 220 mm × 220 mm; matrix size = 64 × 64; slice thickness = 3 mm, slice gap = 1 mm; 35 interleaved axial slices; 185 volumes. Diffusion tensor imaging (DTI) data were acquired using a spin-echo single-shot echo planar imaging (SE-SS-EPI) sequence with the following parameters: TR = 10,000 ms; TE = 74 ms; flip angle = 90 °; FOV = 256 mm × 256 mm; matrix = 128 × 128; slice thickness = 3 mm without gap; 50 axial slices; 64 diffusion gradient directions (b = 1000 s/mm^2) plus five b = 0 reference images. All images were visually inspected to ensure that only images without visible artifacts were included in subsequent analyses.

Structural MRI data analysis

Gray matter morphology was assessed using voxel-based morphometry (VBM) and surface-based morphometry (SBM) analyses. VBM analysis was performed using the CAT12 toolbox (http://www.neuro.uni-jena.de/cat) implemented in the Statistical Parametric Mapping software (SPM12, http://www.fil.ion.ucl.ac.uk/spm). First, all the structural T1-weighted images were corrected for bias-field inhomogeneities. Second, these images were segmented into gray matter, white matter, and cerebrospinal fluid density maps using the "new-segment" approach [53], with total intracranial volume (TIV) obtained. Third, a diffeomorphic anatomical registration through the exponentiated Lie algebra (DARTEL) technique was used to generate a custom, study-specific template [54]. Fourth, each participant's gray matter density image was warped to the customized template; then the resultant images were affine registered to the Montreal Neurological Institute (MNI) space and resampled to a voxel size of 1.5 mm × 1.5 mm × 1.5 mm. Fifth, the modulation was applied by multiplying the transformed gray matter density maps with the non-linear components of Jacobian determinants, which resulted in normalized gray matter volume (GMV) maps. An automated anatomical labeling (AAL) template was employed to segment the cerebrum into 90 cortical and subcortical regions [55]. Mean GMV within each brain region was extracted for subsequent analysis.

SBM analysis was performed using the surface-preprocessing pipeline of the CAT12 toolbox. We used a projection-based thickness estimation that allows the calculation of cortical thickness (CT) and the central surface [25]. For the estimation of white matter distances, we subjected the T1-weighted images to tissue segmentation. Local maxima were then projected to other gray matter voxels by using a neighbor relationship described by the white matter distance. These values equal CT. This projection-based approach also included partial volume correction and correction for sulcal blurring and asymmetries. Topological correction was carried out through a method based on spherical harmonics. For reparametrization of the surfaces, an algorithm for spherical mapping of the cortical surface was applied [56]. An adapted two-dimensional DARTEL algorithm [54] was then applied to the surface for spherical registration. Desikan-Killiany atlas was utilized to parcellate the cerebral cortex into 68 regions. Mean CT within each cortical region was extracted.

fMRI data analysis

Resting-state fMRI data were preprocessed using SPM12 and Data Processing & Analysis for Brain Imaging (DPABI, http://rfmri.org/dpabi) [57] according to a validated pipeline [58–60]. The first 10 volumes for each participant were discarded to allow the signal to reach equilibrium and the participants to adapt to the scanning noise. The remaining volumes were corrected for the acquisition time delay between slices. Then, realignment was performed to correct the motion between time points. Head motion parameters were computed by estimating the translation in each direction and the angular rotation on each axis for each volume. All participants' data were within the defined motion thresholds (i.e., translational or rotational motion parameters less than 3 mm or 3 °). We also calculated frame-wise displacement (FD), which indexes the volume-to-volume changes in head position. Several nuisance covariates (the linear drift, the estimated motion parameters based on the Friston-24 model, the spike volumes with FD > 0.5 mm, the white matter signal, and the cerebrospinal fluid signal) were regressed out from the data. Notably, we did not perform global signal regression since it is still a controversial topic in resting-state fMRI analysis [61]. The datasets were then band-pass filtered using a frequency range of 0.01–0.1 Hz. In the normalization step, individual structural images were firstly co-registered with the mean functional images; then the transformed structural images were segmented and normalized to the MNI space using the DARTEL technique [54]. Finally, each filtered functional volume was spatially normalized to the MNI space using the deformation parameters estimated during the above step and resampled into a 3-mm cubic voxel.

Three resting-state fMRI measures reflecting spontaneous intrinsic brain activity were calculated in the following way. (1) The BOLD time course of each voxel obtained from the preprocessed fMRI data without band-pass filtering was transformed to a frequency

domain via a Fast Fourier Transform, and then the power spectrum was obtained. Fractional amplitude of low-frequency fluctuations (fALFF) was defined as the ratio of the power spectrum in the low-frequency band (0.01–0.1 Hz) to that in the entire frequency range [27]. (2) Regional homogeneity (ReHo) was calculated as the Kendall's coefficient of concordance of the time course of a given voxel with those of its nearest neighbours (26 voxels) [28, 31]. (3) Pearson's correlation coefficients were calculated between the BOLD time courses of all pairs of voxels and a whole-brain functional connectivity matrix was obtained for each participant. For a given voxel, functional connectivity density (FCD) was defined as the number of functional connections with correlation coefficients above a threshold of 0.25 between that voxel and all other voxels within the whole brain [29, 62, 63]. For these fMRI measures, the value of each voxel was divided by the global mean value within the whole brain, yielding standardized fALFF, ReHo, and FCD maps. Mean fALFF, ReHo, and FCD within each brain region of the AAL template were extracted.

DTI data analysis

For DTI data, standard processing steps were performed by using the FMRIB Software Library (FSL, www.fmrib.ox.ac.uk/fsl). First, eddy current distortion and head motion were corrected by registering the diffusion-weighted images to the first b0 image through the affine transformations. Second, the data were skull-stripped by using the FMRIB Brain Extraction Tool. Finally, fractional anisotropy (FA) was calculated to evaluate white matter integrity by using the DTIFIT toolbox. Then, the tract-based spatial statistics pipeline was conducted [30]. Briefly, individual FA images were firstly non-linearly registered to the MNI space. After transformation into the MNI space, mean FA image was created and thinned to generate a mean FA skeleton. Then, each subject's FA image was projected onto the skeleton via filling the mean FA skeleton with FA values from the nearest relevant tract center by searching perpendicular to the local skeleton structure for maximum FA value. Finally, the Johns Hopkins University probabilistic white matter atlas was used to define 50 white matter tracts in the whole brain [64]. Mean FA within each tract was extracted.

Statistical analysis

Demographic, clinical, cognitive, gut microbiome, fecal metabolome, and multi-modal MRI data were analyzed with the SPSS 23.0 software (SPSS, Chicago, Ill) and MetaboAnalyst 5.0 (https://www.metaboanalyst.ca) [65]. First, demographic, clinical, and cognitive data were compared across three groups using one-way analysis of variance (ANOVA) for continuous and Pearson's chi-squared test for categorical variables. Second, we adopted a multi-stage approach to examine group differences in gut microbiome. Kruskal Wallis test was used to compare alpha diversity indices. For beta diversity, a combination of principal coordinate analysis (PCoA) and permutational multivariate analysis of variance (PERMANOVA) was used to test group difference in gut microbial composition. To determine the exact taxa contributing to the microbial composition difference, microbial relative abundance at the genus level was residualized for confounding factors (age, sex, years of education, BMI, current smoking, alcohol abuse, and comorbidities) using the 'fitlm' function in MATLAB and then compared using Kruskal Wallis test. Third, quantification values of fecal metabolites were residualized for the same confounders and then compared across three groups using one-way ANOVA. Fourth, multi-modal MRI measures were additionally residualized for modality-specific covariates (TIV for GMV; FD for fALFF, ReHo, and FCD) and then compared using one-way ANOVA. For these analyses, multiple comparison correction was performed using the false discovery rate (FDR) method, with a corrected significance level of $P < 0.05$.

In case of significant group differences in cognition, gut microbiota, fecal metabolites, and neuroimaging measures, we adopted MetaboAnalyst's pattern-matching method [65, 66] to further identify variables showing differences across three groups with a linear, stepwise order from HC to MCI to AD. Multiple testing was corrected by the FDR method.

To establish the relationship among microbiota, metabolites, neuroimaging and cognition, we initially applied principal component analysis (PCA) to the variables showing significant group differences, and 4 first principal components were obtained to represent the common factors of microbiota, metabolites, neuroimaging and cognition, respectively. Subsequently, pattern-matching analysis was performed for these components, and Spearman's correlations were used to examine the associations between these components in all participants. More importantly, to test whether the association between microbiota and cognition was mediated by metabolites and/or neuroimaging, mediation analysis was performed for the 4 first principal components using the PROCESS macro (http://www.processmacro.org/), with microbiota (X) and cognition (Y) as independent and dependent variables, and metabolites (M1) and neuroimaging (M2) as mediating variables. In the mediation model, we sought to establish three pathways: 1) X → M1 → M2 → Y; 2) X → M1 → Y; and 3) X → M2 → Y. All pathways were reported as unstandardized ordinary least squares regression coefficients, namely, total effect of X on Y (c) = indirect effect of X on Y through M1 (a1 × b1) + indirect effect of X on Y through M2 (a2 × b2) + indirect effect of X on Y through M1 and M2 (a1

× d × b2) + direct effect of X on Y (c'). The significance analysis was based on 10,000 bootstrap realizations and a significant indirect effect is indicated when the bootstrap 95% confidence interval (CI) does not include zero.

Results

Demographic, clinical, and cognitive characteristics

This study enrolled 166 participants, comprising 30 patients with AD, 75 individuals with MCI, and 61 HC. Demographic, clinical, and cognitive characteristics are presented in Table 1. There were no significant differences in age, sex or education among three groups. Regarding vascular risk factors, the prevalence of alcohol, smoking, hypertension, diabetes, and hyperlipidemia was comparable across three groups, while BMI showed a significant group difference. With respect to cognition, there were significant group differences in MMSE, MoCA, AVLT-IR, AVLT-SR, AVLT-LR and AVLT-recognition, manifesting as a progressive decline from HC to MCI to AD.

Table 1 Demographic, clinical, and cognitive characteristics of the participants

Characteristic	HC ($N=61$)	MCI ($N=75$)	AD ($N=30$)	Statistical test
Age (years)	62.39 ± 6.92	64.48 ± 7.91	65.47 ± 7.99	$F=2.066$, $P=0.130$
Sex (female)	36 (59.0%)	41 (54.7%)	23 (76.7%)	$\chi^2=4.391$, $P=0.111$
Education (years)	8.57 ± 4.45	8.11 ± 3.39	6.93 ± 4.33	$F=1.714$, $P=0.183$
BMI (kg/m^2)	23.71 ± 2.65	23.12 ± 2.81	21.38 ± 2.34	**$F=7.747$, $P<0.001$**
Alcohol abuse	10 (16.4%)	17 (22.7%)	6 (20.0%)	$\chi^2=0.831$, $P=0.660$
Current smoking	10 (16.4%)	19 (25.3%)	4 (13.3%)	$\chi^2=2.673$, $P=0.263$
Hypertension	14 (23.0%)	27 (36.0%)	11 (36.7%)	$\chi^2=3.148$, $P=0.207$
Diabetes mellitus	6 (9.8%)	10 (13.3%)	5 (16.7%)	$\chi^2=0.907$, $P=0.635$
Dyslipidemia	13 (21.3%)	13 (17.3%)	6 (20.0%)	$\chi^2=0.354$, $P=0.838$
MMSE	28.67 ± 1.39	25.83 ± 2.71	14.70 ± 6.23	**$F=184.913$, $P<0.001$**
MoCA	25.82 ± 2.53	19.81 ± 3.16	9.40 ± 4.54	**$F=236.927$, $P<0.001$**
AVLT-IR	16.66 ± 4.16	13.40 ± 4.15	6.43 ± 5.08	**$F=44.933$, $P<0.001$**
AVLT-SR	5.98 ± 2.10	3.94 ± 2.20	1.16 ± 1.57	**$F=41.736$, $P<0.001$**
AVLT-LR	5.47 ± 2.21	3.36 ± 2.26	0.42 ± 0.96	**$F=43.962$, $P<0.001$**
AVLT-recognition	21.43 ± 2.40	19.15 ± 2.77	12.35 ± 6.373	**$F=52.095$, $P<0.001$**

Data are expressed as n (%) or mean ± standard deviation. One-way ANOVA (F) and Pearson's chi-squared tests (χ^2) were conducted for continuous and categorical variables, respectively. Entries in bold indicate a significant difference between groups. Abbreviations: AD, Alzheimer's disease; ANOVA, analysis of variance; AVLT-IR, auditory verbal learning test immediate recall; AVLT-SR, auditory verbal learning test short term recall; AVLT-LR, auditory verbal learning test long term recall; BMI, body mass index; HC, healthy controls; MCI, mild cognitive impairment; MMSE, Mini-Mental State Examination; MoCA, Montreal Cognitive Assessment

Gut microbiome in the AD continuum

Alpha diversity analysis demonstrated no significant differences in Shannon and Simpson indices among three groups (Fig. 1A and Supplementary File 1). Beta diversity analysis revealed significant differences in gut microbial composition between AD and the other two groups based on Bray-Curtis index (PERMANOVA, AD vs. HC: $P=1.50\times10^{-3}$, AD vs. MCI: $P=4.32\times10^{-3}$, FDR corrected) and weighted UniFrac distance (PERMANOVA, AD vs. HC: $P=3.37\times10^{-3}$, AD vs. MCI: $P=9.00\times10^{-3}$, FDR corrected), but no significant differences between MCI and HC (Fig. 1B and Supplementary File 2).

HC, MCI, and AD showed similar group-average microbial composition at the genus level, with the dominant bacteria including Phocaeicola, Faecalibacterium, Paraburkholderia, Bacteroides, Pseudomonas, Blautia, Pseudescherichia, Roseburia, Prevotella, and Ruminococcus (Fig. 1C). However, Kruskal Wallis test revealed significant differences in relative abundance of 10 microbial taxa among three groups ($P<0.05$, FDR corrected) (Supplementary File 3). Further pattern-matching analysis demonstrated that 8 microbial taxa (Sphingomonas, Staphylococcus, Stenotrophomonas, Massilia, Variovorax, Bacillus, Bosea, and Dyella) exhibited a progressive increase from HC to MCI to AD, and 2 taxa (Limosilactobacillus and Anaerostipes) showed a gradual decrease ($P<0.05$, FDR corrected) (Supplementary File 3). Box plots of relative abundance of the representative microbial taxa in three groups are illustrated in Fig. 1D.

Fecal metabolome in the AD continuum

After quality control, data filtering and normalization, a total of 505 fecal metabolites were obtained. One-way ANOVA revealed significant differences in quantification values of 27 fecal metabolites across three groups ($P<0.05$, FDR corrected) (Supplementary File 4). Further pattern-matching analysis demonstrated that 26 metabolites showed a progressive increase from HC to MCI to AD, including Arachidonic, Adrenic, and Lithocholic acids, among others ($P<0.05$, FDR corrected) (Supplementary File 4). Box plots of quantification values of the representative fecal metabolites in three groups are illustrated in Fig. 2.

Brain abnormalities in the AD continuum

Results of group comparisons in multi-modal MRI measures are provided in Supplementary File 5. One-way ANOVA revealed significant group differences in GMV

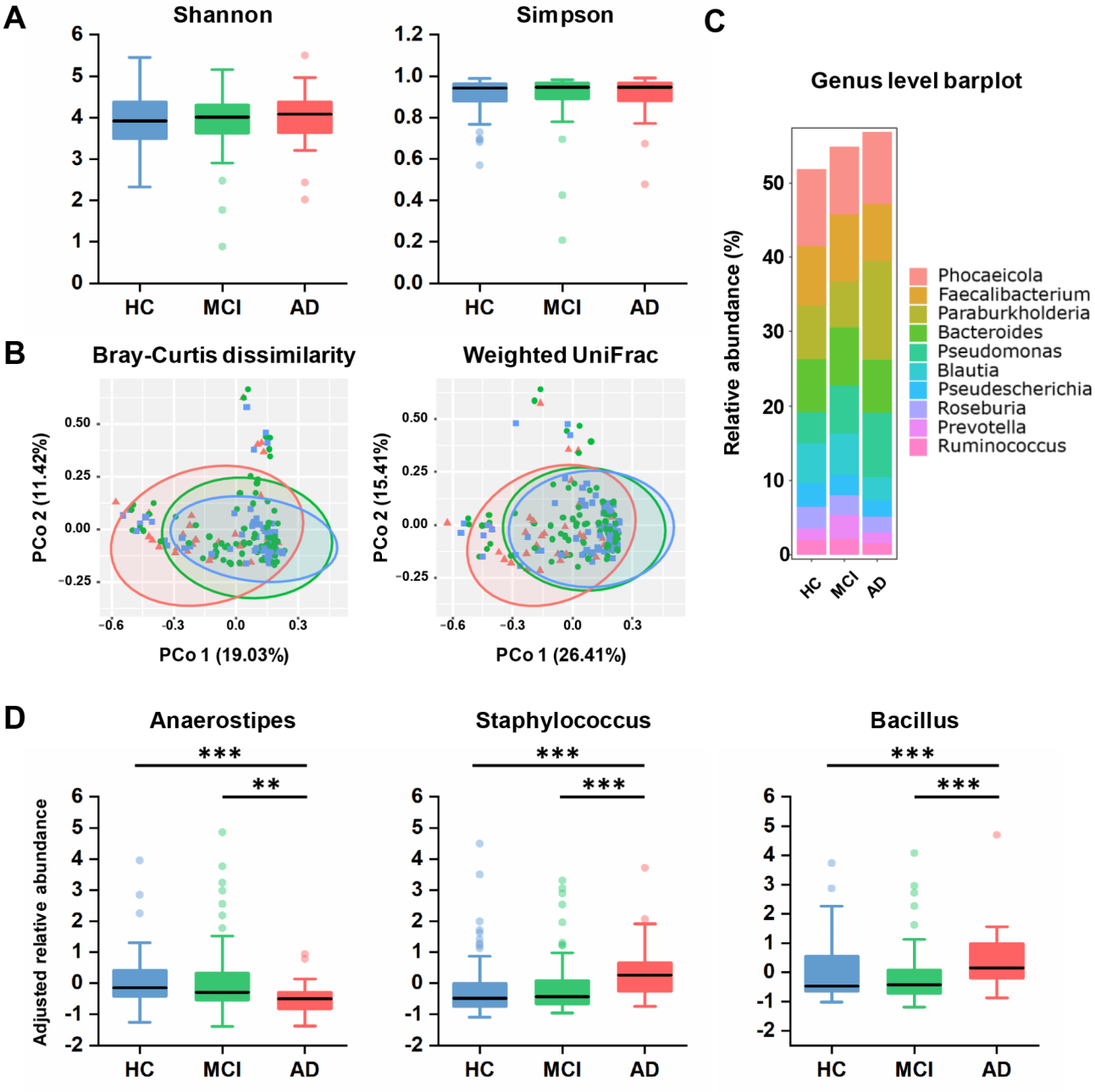

Fig. 1 Gut microbiome in the AD continuum. (**A**) Box plots of alpha diversity using Shannon and Simpson indices. Each box plot shows the median, interquartile range, minimum, and maximum. (**B**) PCoA plots of beta diversity using Bray-Curtis index and weighted UniFrac distance. The axes represent the two dimensions explaining the greatest proportion of variance in microbial composition. Each symbol represents a sample. (**C**) Bar plot of group-average dominant microbial composition at the genus level. (**D**) Box plots of relative abundance of the representative microbial taxa with significant group differences at the genus level. Staphylococcus and Bacillus exhibited a progressive increase from HC to MCI to AD, and Anaerostipes showed a progressive decrease. The asterisks reflect the statistical significance of the pairwise comparisons. *$P<0.05$, **$P<0.01$, ***$P<0.001$. Abbreviations: AD, Alzheimer's disease; HC, healthy controls; MCI, mild cognitive impairment; PCoA, principal coordinate analysis

across a widely distributed set of 74 Gy matter regions ($P<0.05$, FDR corrected). Further pattern-matching analysis demonstrated a progressive GMV reduction from HC to MCI to AD in 63 regions ($P<0.05$, FDR corrected) (Fig. 3A). This was also the case for the CT analysis, with 47 cortical regions showing group differences and 42 regions showing a progressive CT reduction (Fig. 3B). Contrasting with the widespread nature of structural changes, gray matter functional alterations in the AD continuum were less extensive or non-significant. There

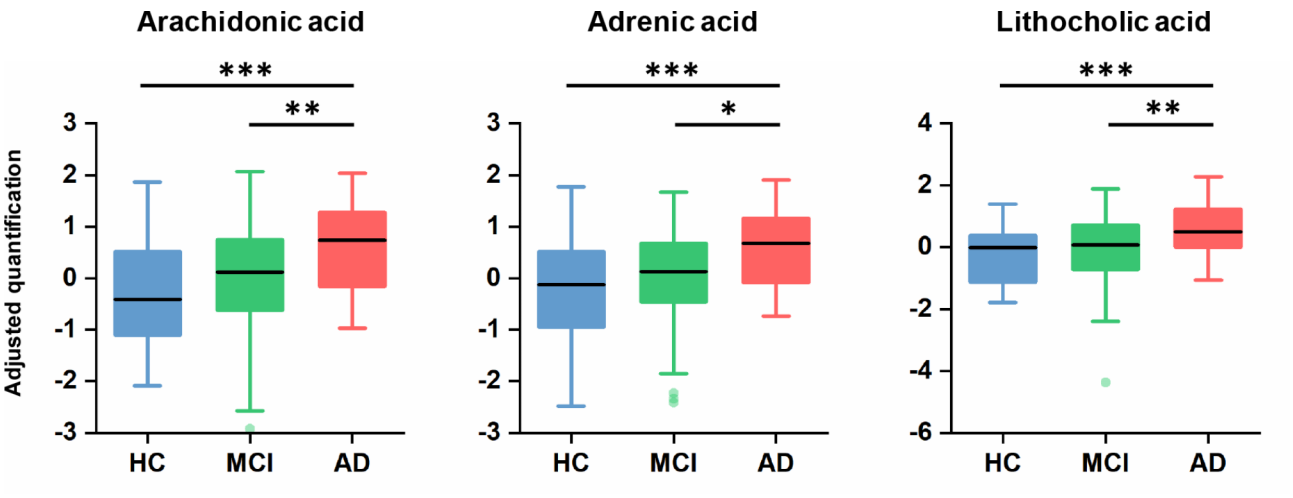

Fig. 2 Fecal metabolome in the AD continuum. Box plots of quantification values of the representative fecal metabolites with significant group differences. Quantification values of Arachidonic, Adrenic, and Lithocholic acids showed a progressive increase from HC to MCI to AD. The asterisks reflect the statistical significance of the pairwise comparisons. *$P < 0.05$, **$P < 0.01$, ***$P < 0.001$. Abbreviations: AD, Alzheimer's disease; HC, healthy controls; MCI, mild cognitive impairment

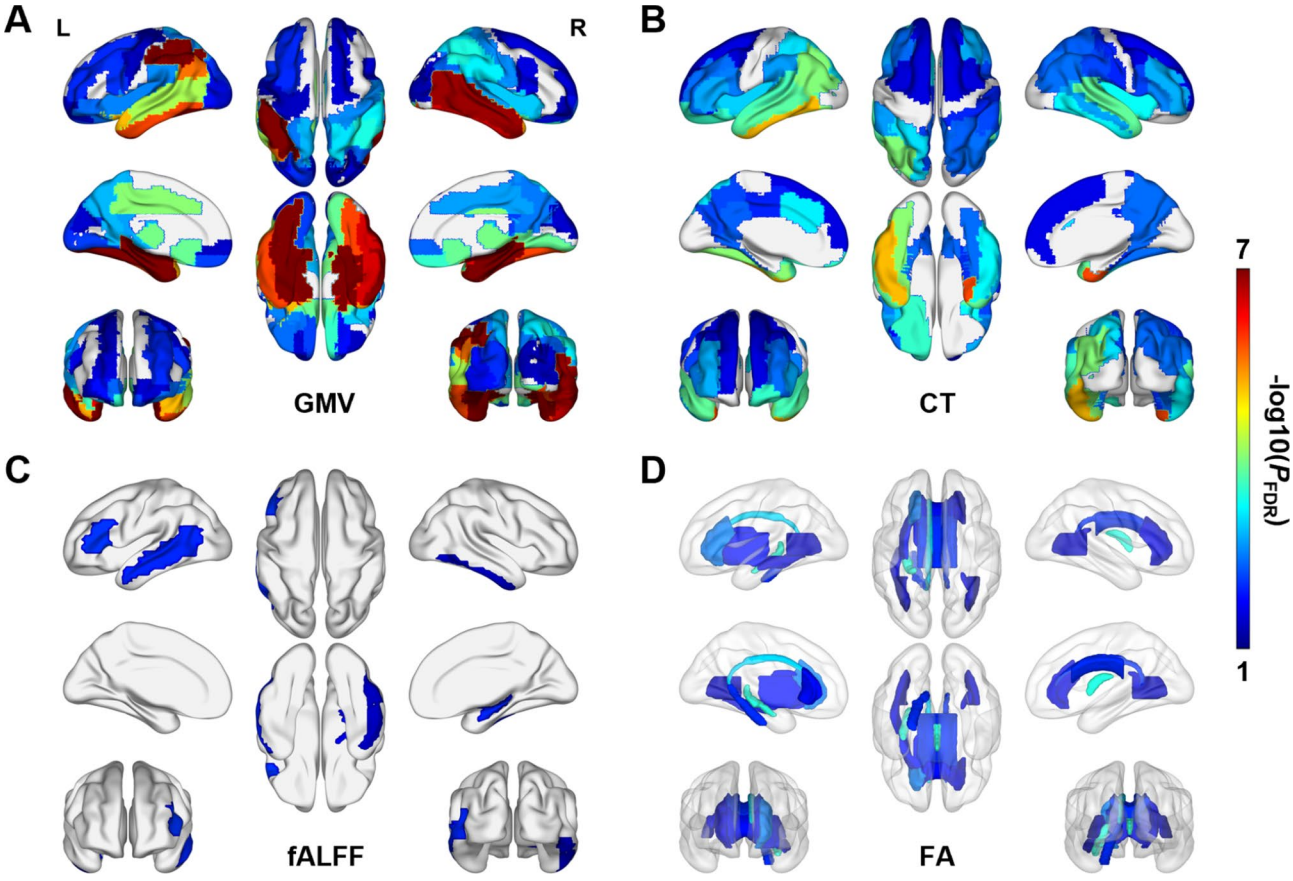

Fig. 3 Brain abnormalities in the AD continuum. GMV (**A**), CT (**B**), fALFF (**C**), and FA (**D**) differences across three groups with a linear, stepwise order from HC to MCI to AD. Color bar indicates -log10(P_{FDR}) in pattern-matching analysis. Abbreviations: AD, Alzheimer's disease; CT, cortical thickness; FA, fractional anisotropy; fALFF, fractional amplitude of low-frequency fluctuations; FDR, false discovery rate; GMV, gray matter volume; HC, healthy controls; L, left; MCI, mild cognitive impairment; R, right

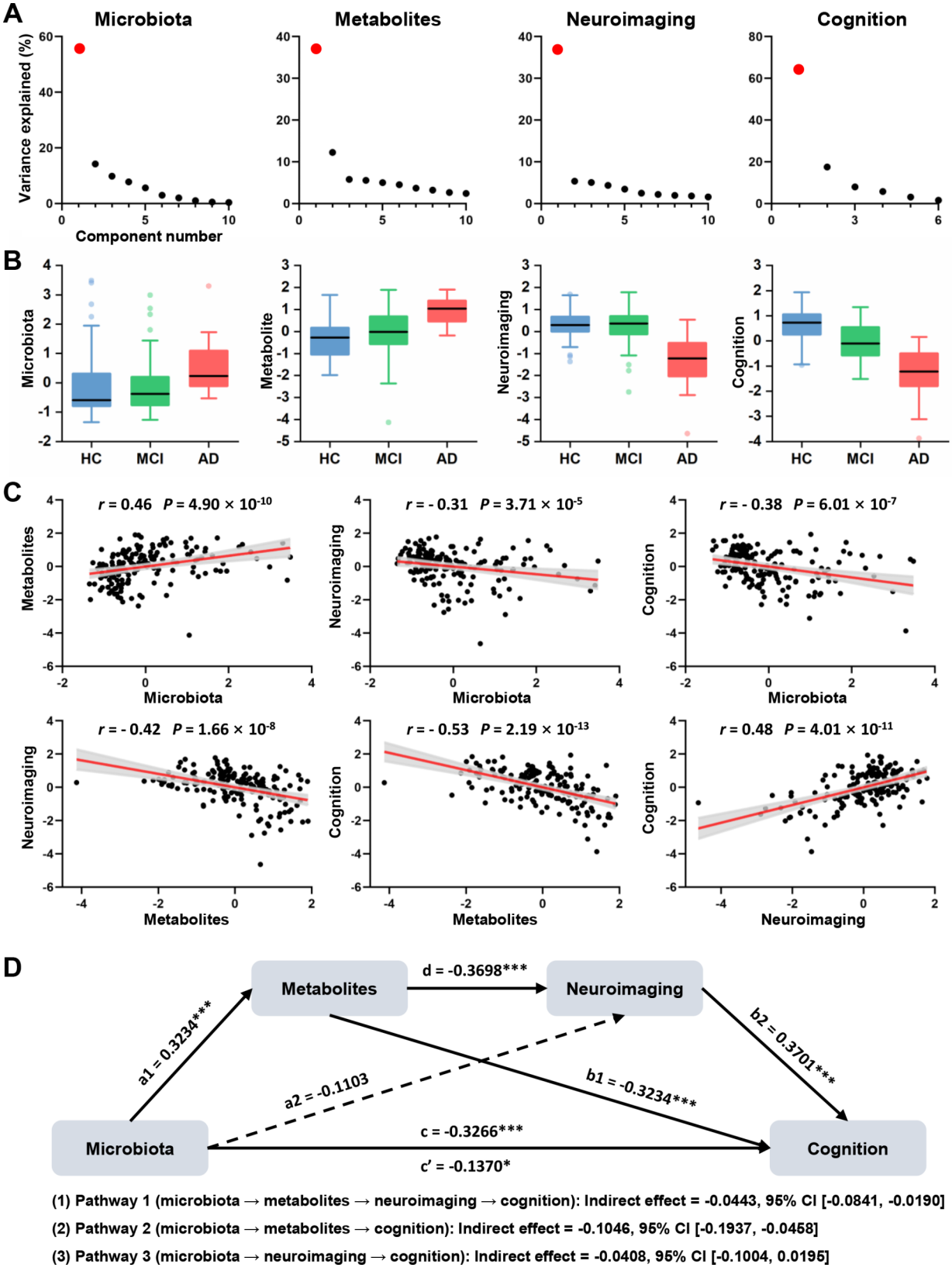

Fig. 4 (See legend on next page.)

(See figure on previous page.)

Fig. 4 Associations between gut microbiota, fecal metabolites, neuroimaging, and cognition. (**A**) Variance explained by the principal components in microbiota, metabolites, neuroimaging, and cognition. (**B**) Box plots of the four first principal components showing a progressive increase from HC to MCI to AD for microbiota and metabolites, and a progressive decrease for neuroimaging and cognition. (**C**) Scatter plots of Spearman's correlations between the four first principal components, representing associations between microbiota, metabolites, neuroimaging, and cognition in all participants. (**D**) Mediation analysis of these components identified two potential mediation pathways: (1) microbiota → metabolites → neuroimaging → cognition, and (2) microbiota → metabolites → cognition. However, the microbiota → neuroimaging → cognition pathway was not significant. *$P < 0.05$, **$P < 0.01$, ***$P < 0.001$. Abbreviations: AD, Alzheimer's disease; CI, confidence interval; HC, healthy controls; MCI, mild cognitive impairment

were significant differences in fALFF in 4 Gy matter regions; among these regions, the left triangular part of inferior frontal gyrus, middle temporal gyrus, and right hippocampus exhibited a gradual fALFF decrease from HC to MCI to AD, and the right inferior temporal gyrus showed a progressive increase (Fig. 3C). As to ReHo and FCD, no significant results were observed. In addition, white matter integrity was broadly affected in the AD continuum, characterized by 21 white matter tracts exhibiting group differences in FA and 15 tracts showing a gradual FA reduction from HC to MCI to AD (Fig. 3D).

Associations between microbiota, metabolites, neuroimaging, and cognition

PCA revealed that the first principal components, accounting for the greatest variance (microbiota: 56%, metabolites: 37%, neuroimaging: 37%, and cognition: 64%), could represent the common factors of microbiota, metabolites, neuroimaging and cognition, respectively (Fig. 4A). Pattern-matching analysis of the four first principal components demonstrated a progressive increase from HC to MCI to AD for microbiota and metabolites, and a progressive decrease for neuroimaging and cognition ($P < 0.05$, FDR corrected) (Fig. 4B). Spearman's correlation analysis revealed significant associations between the four first principal components in all participants (Fig. 4C). Of more importance, further mediation analysis of these components identified two potential mediation pathways: (1) microbiota → metabolites → neuroimaging → cognition, and (2) microbiota → metabolites → cognition. That said, the relationship between microbiota and cognition was significantly mediated by metabolites and neuroimaging (indirect effect = -0.0443, 95% CI: -0.0841, -0.0190) or by metabolites alone (indirect effect = -0.1046, 95% CI: -0.1937, -0.0458) (Fig. 4D). However, no significant mediation effect of neuroimaging alone on the relationship between microbiota and cognition (microbiota → neuroimaging → cognition) was observed (indirect effect = -0.0408, 95% CI: -0.1004, 0.0195).

Discussion

By using a combination of 16S rDNA amplicon sequencing, untargeted metabolomics, and multi-modal MRI, this is the first study comprehensively investigating microbiota-metabolites-brain-cognition pathways in the AD continuum. Gut microbiomics analysis in AD, MCI and HC revealed no significant difference in alpha diversity among three groups, while there were significant group differences in gut microbial composition, which were driven by 8 microbial taxa exhibiting a progressive increase (e.g., Staphylococcus and Bacillus) in relative abundance from HC to MCI to AD, and 2 taxa (e.g., Anaerostipes) showing a gradual decrease. Fecal metabolomics analysis demonstrated that 26 metabolites (e.g., Arachidonic, Adrenic, and Lithocholic acids) exhibited a progressive increase from HC to MCI to AD. Multi-modal MRI analysis also showed progressive gray matter atrophy in broadly distributed gray matter regions and gradual micro-structural integrity damage in widespread white matter tracts along the AD continuum. Integration of these multi-omics changes revealed significant associations between microbiota, metabolites, neuroimaging, and cognition. More importantly, mediation analysis identified two potential mediation pathways: (1) microbiota → metabolites → neuroimaging → cognition, and (2) microbiota → metabolites → cognition. Aside from elucidating the underlying mechanism whereby gut microbiota dysbiosis is linked to AD, our findings may contribute to groundwork for future interventions targeting the microbiota-metabolites-brain-cognition pathways as a therapeutic strategy in the AD continuum.

Despite no difference in alpha diversity across AD, MCI and HC, beta diversity analysis revealed significant group differences in gut microbial composition between AD and the other two groups. Further microbial abundance analysis demonstrated that the microbial composition differences were mainly driven by specific microbial taxa showing progressive alterations from HC to MCI to AD, which is coherent with earlier reports [13, 67–69]. These findings jointly work to endorse the notion that gut microbiota dysbiosis may occur at the early stage of dementia and presents a gradual deterioration during disease progression. Among the affected microbial taxa, Anaerostipes, Staphylococcus and Bacillus may serve as particularly appropriate examples to disentangle the relationship between gut microbiota dysbiosis and AD. Anaerostipes possesses the ability to utilize dietary inositol for the production of short chain fatty acids (SCFAs), which beneficially modulate the peripheral and central nervous systems [70]. Decreased Anaerostipes might give rise to reduced SCFAs, which have been suggested to play a critical role in AD [71]. Indeed, previous work has indicated that SCFAs are decreased in the faeces and the serum from AD patients' fecal transplanted germ-free

mice, which may lead to a disruption in blood-brain barrier homeostasis and innate immune and glial activation [72, 73]. There is mounting evidence supporting the idea that AD can be caused by microbial infections [74–76]. Compatible with this view, we observed an increase in Staphylococcus and Bacillus in the AD continuum. It has been evident that Staphylococcus and Bacillus could produce functional bacterial amyloid proteins [77, 78]. Functional bacterial amyloid proteins are associated with AD by cross-seeding of amyloid misfolding, altered proteostasis, and oxidative stress [79]. Moreover, Staphylococcaceae exhibited higher levels in AD brains than in control brains [76]. These data invite the speculation that increase in specific pathogenic bacteria may contribute to the pathogenesis and/or progression of AD [76].

Fecal metabolomics analysis demonstrated that 26 metabolites exhibited a progressive increase from HC to MCI to AD. Among the affected metabolites, Arachidonic, Adrenic, and Lithocholic acids are thought to be prominently involved in the pathophysiology of AD. Arachidonic acid is a poly-unsaturated fatty acid that is of vital importance for human health. Oxidative Arachidonic acid metabolism is a major hallmark of neuroinflammation [80], which may explain the intimate link between lipid metabolism and Alzheimer's disease [81, 82]. In addition, Arachidonic acid functions as a critical mediator in Aβ-induced pathogenesis, leading to learning, memory, and behavioral impairments in mouse models of AD [81]. Adrenic acid is an endogenously synthesized polyunsaturated free fatty acid [83]. Abnormal metabolism of Arachidonic and Adrenic acids can trigger the activation of ferroptosis [84–86], a form of cell death driven by iron-dependent lipid peroxidation [87]. The involvement of ferroptosis in neurodegenerative diseases including Alzheimer's disease has been well documented [88, 89]. Lithocholic acid is a secondary bile acid, which is synthesized in the colon by intestinal bacteria from chenodeoxycholic acid [90, 91]. Marksteiner et al. reported that levels of Lithocholic acid were enhanced in AD relative to HC, and Lithocholic acid could act as a useful biomarker to separate AD from HC [90]. Broadly, solid evidence has suggested that altered bile acid profile associates with cognitive impairment in Alzheimer's disease [92, 93].

Multi-modal MRI techniques offer us sufficient material to attempt a more thorough characterization of brain structural and functional changes in the AD continuum [21, 94–96]. We found progressive gray matter atrophy in broadly distributed gray matter regions and gradual micro-structural integrity damage in widespread white matter tracts along the AD continuum. In accordance with our observation, extensive research has shown that gray matter atrophy affects very early the medial temporal lobe, entorhinal cortex and hippocampus, soon after extending to the remainder of the cortex along a temporal-parietal-frontal trajectory, while motor areas are generally spared until late disease stages [97–103]. Correspondingly, tau accumulation is most frequently observed in the medial temporal regions and stepwise spreads to the basal and lateral temporal, inferior parietal, posterior cingulate, and the other association cortices, and then ultimately to the primary cortical regions [104]. In addition, numerous DTI studies have documented widespread white matter integrity impairment in AD and MCI [105–109], which is consistent with our finding. Moreover, longitudinal studies in MCI and AD patients have suggested that white matter integrity represents an indicator of disease progression [110, 111].

The relations between the gut microbiota and cognitive functions in the AD continuum have been clearly established. For example, altered gut microbiota in adults with subjective cognitive decline was found to associate with cognitive performance [69]. Correlations between gut microbial abundance and cognitive deficits have been observed in MCI and AD patients [13, 67, 68, 112]. In parallel, there has been increasing interest in investigating the associations between metabolites and cognitive functions in AD. For instance, altered bile acid profile was found to associate with cognitive decline in AD [93]. Wu et al. identified differences between AD and HC in tryptophan metabolites, SCFAs, and lithocholic acid, the majority of which correlated with altered microbiota and cognitive impairment [113]. Jiang et al. reported that concentrations of several blood metabolites, including lipids, amino acids, and steroids were associated with cognitive decline and the incidence or progression of dementia [114]. Complementing and extending these prior findings, our mediation analysis identified two potential mediation pathways: (1) microbiota → metabolites → neuroimaging → cognition, and (2) microbiota → metabolites → cognition. Theoretically, these findings may add important context to the growing literature on the effects of gut microbiome on cognition in the AD continuum by shedding light on the molecular and neuropathological mechanisms underlying such effects. More broadly, our results may expose the gut microbiota as a new therapeutic target for improving cognitive impairment in the AD continuum, which may be of high clinical and translational importance.

Our study has several limitations that should be mentioned. First, the diagnosis of MCI and AD was based on clinical symptoms and routine neuroimaging signatures in this study. Reliable AD biomarkers should be included to aid in accurate diagnosis in future studies. Second, the correlational design of this investigation means that further longitudinal and mechanistic research must be conducted to determine the causative nature of the multi-omics associations. Third, we performed a

PCA to reduce the dimensionality of the variables and selected 4 first principal components to represent the common factors of microbiota, metabolites, neuroimaging and cognition. Although some information may be lost, principal components with potential biological relevance tend to be more tractable than working with the high-dimensional original data. Fourth, while mediation analysis was a key focus of our work and allowed us to identify the pathways from microbiota to cognition, we must acknowledge that mediation analysis has its own limitations. Specifically, mediation analysis, a regression-based approach, examines the relationship between variables and can suggest potential pathways, but it cannot establish directionality of the pathways [115, 116]. The specification of independent and dependent variables is often based on our existing knowledge and assumptions, which may not fully capture the complexity of biological interactions. Other potential pathways, such as those from cognition to microbiota, are of great interest and merit further research in our future work. Finally, we performed our analysis without controlling for oral probiotics or yogurt that would influence the gut microbiota. For one, participants who took oral probiotics or yogurt were randomly distributed across the sample, such that it is unlikely that these participants would affect the analysis in a systematic manner. For another, substantial variability in use frequency, amount, and types makes it challenging to precisely quantify this factor.

Conclusions

In summary, our multi-omics data established plausible microbiota-metabolites-brain-cognition pathways in the AD continuum, which may illuminate the underlying mechanisms whereby gut microbiota dysbiosis is linked to AD. More generally, our findings might have important clinical implications for developing treatment approaches targeting the microbiota-metabolites-brain-cognition pathways in the AD continuum.

Abbreviations

AD	Alzheimer's disease
MCI	Mild cognitive impairment
HC	Healthy controls
NIA-AA	National Institute on Aging Alzheimer's Association
MoCA	Montreal Cognitive Assessment
MMSE	Mini-Mental State Examination
CDR	Clinical Dementia Rating
BMI	Body mass index
AVLT-IR	Auditory verbal learning test immediate recall
AVLT-SR	Auditory verbal learning test short term recall
AVLT-LR	Auditory verbal learning test long term recall
PCoA	Principal coordinate analysis
CT	Cortical thickness
FA	Fractional anisotropy
fALFF	Fractional amplitude of low-frequency fluctuations
FDR	False discovery rate
GMV	Gray matter volume
CI	Confidence interval
MRI	Magnetic resonance imaging
ASV	Amplicon sequence variants

Supplementary Information

The online version contains supplementary material available at https://doi.org/10.1186/s13195-025-01683-0.

Supplementary Material 1

Supplementary Material 2

Supplementary Material 3

Supplementary Material 4

Supplementary Material 5

Acknowledgements

We thank the subjects who contributed to this study.

Author contributions

H. Z.: Conceptualization, Methodology, Investigation, Formal analysis, Visualization, Data curation, Writing-original draft; X. Z.: Conceptualization, Methodology, Investigation, Visualization, Data curation; Y. S.: Conceptualization, Methodology, Investigation, Visualization; W. Z.: Visualization, Data curation; Z. S.: Conceptualization, Supervision, Project administration; Resources; J. Z.: Conceptualization, Supervision, Project administration; Resources, Writing-review & editing; Y. Y.: Conceptualization, Methodology, Investigation, Supervision, Resources, Funding acquisition. All authors reviewed the manuscript.

Funding

This work was supported by the National Natural Science Foundation of China (grant numbers: 82471952, 82371928 and 82071905), the Anhui Provincial Natural Science Foundation (grant number: 2308085MH277), the Scientific Research Key Project of Anhui Province Universities (grant number: 2022AH051135), the Scientific Research Foundation of Anhui Medical University (grant number: 2022xkj143), and the Postgraduate Innovation Research and Practice Program of Anhui Medical University (grant number: YJS20230012).

Data availability

The dataset generated and analyzed in the current study is available from the corresponding author on reasonable request.

Declarations

Ethics approval and consent to participate

This study was approved by the Institutional Ethics Committee of The First Affiliated Hospital of Anhui Medical University (20200094) and was conducted following the Declaration of Helsinki. Written informed consent was obtained from all participants after a full explanation of the procedure.

Consent for publication

Not applicable.

Competing interests

The authors declare no competing interests.

Author details

[1]Department of Radiology, The First Affiliated Hospital of Anhui Medical University, Hefei 230022, China
[2]Research Center of Clinical Medical Imaging, Anhui Province Hefei 230032, China
[3]Anhui Provincial Institute of Translational Medicine, Hefei 230032, China
[4]Anhui Provincial Key Laboratory for Brain Bank Construction and Resource Utilization, Hefei 230032, China
[5]Department of Neurology, The First Affiliated Hospital of Anhui Medical University, Hefei 230022, China

Received: 6 May 2024 / Accepted: 22 January 2025

Published online: 01 February 2025

References

1. Long JM, Holtzman DM. Alzheimer Disease: an update on pathobiology and treatment strategies. Cell. 2019;179(2):312–39.
2. Lynch SV, Pedersen O. The human intestinal microbiome in Health and Disease. N Engl J Med. 2016;375(24):2369–79.
3. Michaudel C, Sokol H. The gut microbiota at the service of Immunometabolism. Cell Metab. 2020;32(4):514–23.
4. Wu J, et al. The role of the gut microbiome and its metabolites in metabolic diseases. Protein Cell. 2021;12(5):360–73.
5. Jiang C, et al. The gut microbiota and Alzheimer's Disease. J Alzheimers Dis. 2017;58(1):1–15.
6. Chandra S, Sisodia SS, Vassar RJ. The gut microbiome in Alzheimer's disease: what we know and what remains to be explored. Mol Neurodegener. 2023;18(1):9.
7. Minter MR, et al. Antibiotic-induced perturbations in gut microbial diversity influences neuro-inflammation and amyloidosis in a murine model of Alzheimer's disease. Sci Rep. 2016;6:30028.
8. Minter MR, et al. Antibiotic-induced perturbations in microbial diversity during post-natal development alters amyloid pathology in an aged APP(SWE)/PS1(ΔE9) murine model of Alzheimer's disease. Sci Rep. 2017;7(1):10411.
9. Dodiya HB, et al. Sex-specific effects of microbiome perturbations on cerebral Aβ amyloidosis and microglia phenotypes. J Exp Med. 2019;216(7):1542–60.
10. Dodiya HB et al. Gut microbiota-driven brain Aβ amyloidosis in mice requires microglia. J Exp Med, 2022. 219(1).
11. Vogt NM, et al. Gut microbiome alterations in Alzheimer's disease. Sci Rep. 2017;7(1):13537.
12. Zhuang ZQ, et al. Gut microbiota is altered in patients with Alzheimer's Disease. J Alzheimers Dis. 2018;63(4):1337–46.
13. Liu P, et al. Altered microbiomes distinguish Alzheimer's disease from amnestic mild cognitive impairment and health in a Chinese cohort. Brain Behav Immun. 2019;80:633–43.
14. Zierer J, et al. The fecal metabolome as a functional readout of the gut microbiome. Nat Genet. 2018;50(6):790–5.
15. Hofer U. Microbiome: B. Fragilis and the brain. Nat Rev Microbiol. 2014;12(2):76–7.
16. Griffin JL, et al. Metabolomics as a tool for cardiac research. Nat Rev Cardiol. 2011;8(11):630–43.
17. Trivedi DK, Hollywood KA, Goodacre R. Metabolomics for the masses: the future of metabolomics in a personalized world. New Horiz Transl Med. 2017;3(6):294–305.
18. Clish CB. Metabolomics: an emerging but powerful tool for precision medicine. Cold Spring Harb Mol Case Stud. 2015;1(1):a000588.
19. Dehghan A, et al. Metabolome-wide association study on ABCA7 indicates a role of ceramide metabolism in Alzheimer's disease. Proc Natl Acad Sci U S A. 2022;119(43):e2206083119.
20. Horgusluoglu E, et al. Integrative metabolomics-genomics approach reveals key metabolic pathways and regulators of Alzheimer's disease. Alzheimers Dement. 2022;18(6):1260–78.
21. Pini L, et al. Brain atrophy in Alzheimer's Disease and aging. Ageing Res Rev. 2016;30:25–48.
22. Chandra A, Dervenoulas G, Politis M. Magnetic resonance imaging in Alzheimer's disease and mild cognitive impairment. J Neurol. 2019;266(6):1293–302.
23. Ibrahim B, et al. Diagnostic power of resting-state fMRI for detection of network connectivity in Alzheimer's disease and mild cognitive impairment: a systematic review. Hum Brain Mapp. 2021;42(9):2941–68.
24. Rathore S, et al. A review on neuroimaging-based classification studies and associated feature extraction methods for Alzheimer's disease and its prodromal stages. NeuroImage. 2017;155:530–48.
25. Dahnke R, Yotter RA, Gaser C. Cortical thickness and central surface estimation. NeuroImage. 2013;65:336–48.
26. Ashburner J, Friston KJ. Voxel-based morphometry–the methods. NeuroImage. 2000;11(6 Pt 1):805–21.
27. Zou QH, et al. An improved approach to detection of amplitude of low-frequency fluctuation (ALFF) for resting-state fMRI: fractional ALFF. J Neurosci Methods. 2008;172(1):137–41.
28. Zang Y, et al. Regional homogeneity approach to fMRI data analysis. NeuroImage. 2004;22(1):394–400.
29. Tomasi D, Volkow ND. Functional connectivity density mapping. Proc Natl Acad Sci U S A. 2010;107(21):9885–90.
30. Smith SM, et al. Tract-based spatial statistics: voxelwise analysis of multi-subject diffusion data. NeuroImage. 2006;31(4):1487–505.
31. Yang Y, et al. Brain structural and functional alterations specific to low sleep efficiency in major depressive disorder. Front Neurosci. 2020;14:50.
32. Zhang C, et al. Neural correlates of the association between depression and high density lipoprotein cholesterol change. J Psychiatr Res. 2020;130:9–18.
33. Zhu J, et al. Altered coupling between resting-state cerebral blood Flow and Functional Connectivity in Schizophrenia. Schizophr Bull. 2017;43(6):1363–74.
34. Liu S, et al. Brain structure and perfusion in relation to serum renal function indexes in healthy young adults. Brain Imaging Behav. 2022;16(3):1014–25.
35. Chen J, et al. Associations of serum liver function markers with brain structure, function, and perfusion in healthy young adults. Front Neurol. 2021;12:606094.
36. McKhann GM, et al. The diagnosis of dementia due to Alzheimer's disease: recommendations from the National Institute on Aging-Alzheimer's Association workgroups on diagnostic guidelines for Alzheimer's disease. Alzheimers Dement. 2011;7(3):263–9.
37. Albert MS, et al. The diagnosis of mild cognitive impairment due to Alzheimer's disease: recommendations from the National Institute on Aging-Alzheimer's Association workgroups on diagnostic guidelines for Alzheimer's disease. Alzheimers Dement. 2011;7(3):270–9.
38. Lu J, et al. Montreal cognitive assessment in detecting cognitive impairment in Chinese elderly individuals: a population-based study. J Geriatr Psychiatry Neurol. 2011;24(4):184–90.
39. Hughes CP, et al. A new clinical scale for the staging of dementia. Br J Psychiatry. 1982;140:566–72.
40. Gmitrowicz A, Kucharska A. [Developmental disorders in the fourth edition of the American classification: diagnostic and statistical manual of mental disorders (DSM IV -- optional book)]. Psychiatr Pol. 1994;28(5):509–21.
41. Folstein M, et al. The meaning of cognitive impairment in the elderly. J Am Geriatr Soc. 1985;33(4):228–35.
42. Nasreddine ZS, et al. The Montreal Cognitive Assessment, MoCA: a brief screening tool for mild cognitive impairment. J Am Geriatr Soc. 2005;53(4):695–9.
43. Guo Q, et al. A comparison study of mild cognitive impairment with 3 memory tests among Chinese individuals. Alzheimer Dis Assoc Disord. 2009;23(3):253–9.
44. Liu YX, et al. A practical guide to amplicon and metagenomic analysis of microbiome data. Protein Cell. 2021;12(5):315–30.
45. Rognes T, et al. VSEARCH: a versatile open source tool for metagenomics. PeerJ. 2016;4:e2584.
46. Lozupone C, et al. UniFrac: an effective distance metric for microbial community comparison. Isme j. 2011;5(2):169–72.
47. Barri T, Dragsted LO. UPLC-ESI-QTOF/MS and multivariate data analysis for blood plasma and serum metabolomics: effect of experimental artefacts and anticoagulant. Anal Chim Acta. 2013;768:118–28.
48. Want EJ, et al. Solvent-dependent metabolite distribution, clustering, and protein extraction for serum profiling with mass spectrometry. Anal Chem. 2006;78(3):743–52.
49. Tsugawa H, et al. MS-DIAL: data-independent MS/MS deconvolution for comprehensive metabolome analysis. Nat Methods. 2015;12(6):523–6.
50. Gadara D, et al. Systematic feature filtering in exploratory metabolomics: application toward Biomarker Discovery. Anal Chem. 2021;93(26):9103–10.
51. Harshfield EL, et al. Metabolomic profiling in small vessel disease identifies multiple associations with disease severity. Brain. 2022;145(7):2461–71.
52. Bijlsma S, et al. Large-scale human metabolomics studies: a strategy for data (pre-) processing and validation. Anal Chem. 2006;78(2):567–74.
53. Ashburner J, Friston KJ. Unified segmentation. NeuroImage. 2005;26(3):839–51.
54. Ashburner J. A fast diffeomorphic image registration algorithm. NeuroImage. 2007;38(1):95–113.
55. Tzourio-Mazoyer N, et al. Automated anatomical labeling of activations in SPM using a macroscopic anatomical parcellation of the MNI MRI single-subject brain. NeuroImage. 2002;15(1):273–89.
56. Yotter RA, et al. Topological correction of brain surface meshes using spherical harmonics. Hum Brain Mapp. 2011;32(7):1109–24.
57. Yan CG, et al. DPABI: Data Processing & Analysis for (Resting-State) brain imaging. Neuroinformatics. 2016;14(3):339–51.
58. Zhang X, et al. Brain structural and Functional Damage Network Localization of Suicide. Biol Psychiatry. 2024;95(12):1091–9.

59. Cheng Y, et al. Brain Network Localization of Gray Matter Atrophy and Neurocognitive and Social Cognitive Dysfunction in Schizophrenia. Biol Psychiatry; 2024.
60. Mo F, et al. Network Localization of State and Trait of Auditory Verbal Hallucinations in Schizophrenia. Schizophr Bull; 2024.
61. Murphy K, Fox MD. Towards a consensus regarding global signal regression for resting state functional connectivity MRI. NeuroImage. 2017;154:169–73.
62. Zhuo C, et al. Altered resting-state functional connectivity of the cerebellum in schizophrenia. Brain Imaging Behav. 2018;12(2):383–9.
63. Zhuo C, et al. Functional connectivity density alterations in schizophrenia. Front Behav Neurosci. 2014;8:404.
64. Hua K, et al. Tract probability maps in stereotaxic spaces: analyses of white matter anatomy and tract-specific quantification. NeuroImage. 2008;39(1):336–47.
65. Pang Z, et al. MetaboAnalyst 5.0: narrowing the gap between raw spectra and functional insights. Nucleic Acids Res. 2021;49(W1):W388–96.
66. Pavlidis P, Noble WS. Analysis of strain and regional variation in gene expression in mouse brain. Genome Biol, 2001. 2(10): p. Research0042.
67. Li B, et al. Mild cognitive impairment has similar alterations as Alzheimer's disease in gut microbiota. Alzheimers Dement. 2019;15(10):1357–66.
68. Guo M, et al. Gut microbiome features of Chinese patients newly diagnosed with Alzheimer's disease or mild cognitive impairment. J Alzheimers Dis. 2021;80(1):299–310.
69. Sheng C, et al. Altered gut microbiota in adults with subjective cognitive decline: the SILCODE Study. J Alzheimers Dis. 2021;82(2):513–26.
70. Bui TPN, et al. Conversion of dietary inositol into propionate and acetate by commensal Anaerostipes associates with host health. Nat Commun. 2021;12(1):4798.
71. Ho L, et al. Protective roles of intestinal microbiota derived short chain fatty acids in Alzheimer's disease-type beta-amyloid neuropathological mechanisms. Expert Rev Neurother. 2018;18(1):83–90.
72. Chen C, et al. Gut microbiota regulate Alzheimer's disease pathologies and cognitive disorders via PUFA-associated neuroinflammation. Gut. 2022;71(11):2233–52.
73. Silva YP, Bernardi A, Frozza RL. The role of short-chain fatty acids from gut microbiota in Gut-Brain communication. Front Endocrinol (Lausanne). 2020;11:25.
74. Miklossy J. Bacterial amyloid and DNA are important constituents of Senile plaques: further evidence of the spirochetal and Biofilm Nature of Senile plaques. J Alzheimers Dis. 2016;53(4):1459–73.
75. Zhan X, et al. Gram-negative bacterial molecules associate with Alzheimer disease pathology. Neurology. 2016;87(22):2324–32.
76. Alonso R, et al. Infection of Fungi and Bacteria in brain tissue from Elderly persons and patients with Alzheimer's Disease. Front Aging Neurosci. 2018;10:159.
77. Schwartz K, Boles BR. Microbial amyloids–functions and interactions within the host. Curr Opin Microbiol. 2013;16(1):93–9.
78. Friedland RP, McMillan JD, Kurlawala Z. What are the Molecular mechanisms by which functional bacterial amyloids influence amyloid Beta deposition and Neuroinflammation in neurodegenerative disorders? Int J Mol Sci, 2020. 21(5).
79. Friedland RP. Mechanisms of molecular mimicry involving the microbiota in neurodegeneration. J Alzheimers Dis. 2015;45(2):349–62.
80. Farooqui AA, Horrocks LA, Farooqui T. Modulation of inflammation in brain: a matter of fat. J Neurochem. 2007;101(3):577–99.
81. Sanchez-Mejia RO, Mucke L. Phospholipase A2 and arachidonic acid in Alzheimer's disease. Biochim Biophys Acta. 2010;1801(8):784–90.
82. Yin F. Lipid metabolism and Alzheimer's disease: clinical evidence, mechanistic link and therapeutic promise. Febs j. 2023;290(6):1420–53.
83. Hagve TA, Christophersen BO. Evidence for peroxisomal retroconversion of adrenic acid (22:4(n-6)) and docosahexaenoic acids (22:6(n-3)) in isolated liver cells. Biochim Biophys Acta. 1986;875(2):165–73.
84. Dixon SJ, et al. Human haploid cell Genetics reveals roles for lipid metabolism genes in nonapoptotic cell death. ACS Chem Biol. 2015;10(7):1604–9.
85. Doll S, et al. ACSL4 dictates ferroptosis sensitivity by shaping cellular lipid composition. Nat Chem Biol. 2017;13(1):91–8.
86. Kagan VE, et al. Oxidized arachidonic and adrenic PEs navigate cells to ferroptosis. Nat Chem Biol. 2017;13(1):81–90.
87. Stockwell BR. Ferroptosis turns 10: emerging mechanisms, physiological functions, and therapeutic applications. Cell. 2022;185(14):2401–21.
88. Stockwell BR, et al. Ferroptosis: a regulated cell death Nexus linking metabolism, Redox Biology, and Disease. Cell. 2017;171(2):273–85.
89. Reichert CO et al. Ferroptosis mechanisms involved in neurodegenerative diseases. Int J Mol Sci, 2020. 21(22).
90. Marksteiner J, et al. Bile acid quantification of 20 plasma metabolites identifies lithocholic acid as a putative biomarker in Alzheimer's disease. Metabolomics. 2018;14(1):1.
91. Ridlon JM, Kang DJ, Hylemon PB. Bile salt biotransformations by human intestinal bacteria. J Lipid Res. 2006;47(2):241–59.
92. Nho K, et al. Altered bile acid profile in mild cognitive impairment and Alzheimer's disease: relationship to neuroimaging and CSF biomarkers. Alzheimers Dement. 2019;15(2):232–44.
93. MahmoudianDehkordi S, et al. Altered bile acid profile associates with cognitive impairment in Alzheimer's disease-An emerging role for gut microbiome. Alzheimers Dement. 2019;15(1):76–92.
94. Frisoni GB, et al. Detection of grey matter loss in mild Alzheimer's disease with voxel based morphometry. J Neurol Neurosurg Psychiatry. 2002;73(6):657–64.
95. He Y, et al. Regional coherence changes in the early stages of Alzheimer's disease: a combined structural and resting-state functional MRI study. NeuroImage. 2007;35(2):488–500.
96. Medina D, et al. White matter changes in mild cognitive impairment and AD: a diffusion tensor imaging study. Neurobiol Aging. 2006;27(5):663–72.
97. Apostolova LG, et al. Three-dimensional gray matter atrophy mapping in mild cognitive impairment and mild Alzheimer disease. Arch Neurol. 2007;64(10):1489–95.
98. Dickerson BC, et al. The cortical signature of Alzheimer's disease: regionally specific cortical thinning relates to symptom severity in very mild to mild AD dementia and is detectable in asymptomatic amyloid-positive individuals. Cereb Cortex. 2009;19(3):497–510.
99. Frisoni GB, et al. In vivo mapping of incremental cortical atrophy from incipient to overt Alzheimer's disease. J Neurol. 2009;256(6):916–24.
100. Lerch JP, et al. Focal decline of cortical thickness in Alzheimer's disease identified by computational neuroanatomy. Cereb Cortex. 2005;15(7):995–1001.
101. Prestia A, et al. Cortical changes in incipient Alzheimer's disease. J Alzheimers Dis. 2010;22(4):1339–49.
102. Singh V, et al. Spatial patterns of cortical thinning in mild cognitive impairment and Alzheimer's disease. Brain. 2006;129(Pt 11):2885–93.
103. Thompson PM, et al. Dynamics of gray matter loss in Alzheimer's disease. J Neurosci. 2003;23(3):994–1005.
104. Cho H, et al. In vivo cortical spreading pattern of tau and amyloid in the Alzheimer disease spectrum. Ann Neurol. 2016;80(2):247–58.
105. Bosch B, et al. Multiple DTI index analysis in normal aging, amnestic MCI and AD. Relationship with neuropsychological performance. Neurobiol Aging. 2012;33(1):61–74.
106. Huang H, et al. Distinctive disruption patterns of white matter tracts in Alzheimer's disease with full diffusion tensor characterization. Neurobiol Aging. 2012;33(9):2029–45.
107. O'Dwyer L, et al. Multiple indices of diffusion identifies white matter damage in mild cognitive impairment and Alzheimer's disease. PLoS ONE. 2011;6(6):e21745.
108. Pievani M, et al. Assessment of white matter tract damage in mild cognitive impairment and Alzheimer's disease. Hum Brain Mapp. 2010;31(12):1862–75.
109. Stricker NH, et al. Decreased white matter integrity in late-myelinating fiber pathways in Alzheimer's disease supports retrogenesis. NeuroImage. 2009;45(1):10–6.
110. Nowrangi MA, et al. Longitudinal, region-specific course of diffusion tensor imaging measures in mild cognitive impairment and Alzheimer's disease. Alzheimers Dement. 2013;9(5):519–28.
111. Teipel SJ, et al. Longitudinal changes in fiber tract integrity in healthy aging and mild cognitive impairment: a DTI follow-up study. J Alzheimers Dis. 2010;22(2):507–22.
112. Zhu Z et al. Altered Gut Microbiota and Its Clinical Relevance in Mild Cognitive Impairment and Alzheimer's Disease: Shanghai Aging Study and Shanghai Memory Study. Nutrients, 2022. 14(19).
113. Wu L et al. Altered Gut Microbial Metabolites in Amnestic Mild Cognitive Impairment and Alzheimer's Disease: Signals in Host-Microbe Interplay. Nutrients, 2021. 13(1).
114. Jiang Y, et al. Metabolomics in the Development and Progression of Dementia: a systematic review. Front Neurosci. 2019;13:343.
115. Tönnies T, et al. Mediation Analysis in Medical Research. Dtsch Arztebl Int. 2023;120(41):681–7.

116. Rijnhart JJM, et al. Mediation analysis methods used in observational research: a scoping review and recommendations. BMC Med Res Methodol. 2021;21(1):226.

Publisher's note